ARMA 16-571

Role of large scale heterogeneities on in-situ stress and induced stress fields

Kaiser, P.K.
Laurentian University, Sudbury, Ontario, Canada
Maloney, S.M.
MIRARCO – Mining Innovation, Sudbury, Ontario, Canada
Yong, S.
MIRARCO, now Knight Piésold, Vancouver, British Columbia, Canada

ABSTRACT: At ARMA's 2006 symposium, Maloney et al. (2006) presented a "Reassessment of in situ stresses in the Canadian Shield" to assist in establishing representative in-situ stress conditions appropriate for sub-regional modeling activities. A recent updated is available from Yong and Maloney (2015). In this article, it is demonstrated (a) how earth crust straining may affect the in-situ stress profile, (b) how the in-situ stress magnitudes vary in heterogeneous rock masses, and (c) what the consequences are for excavation stability in such variable stress fields. The first two points are discussed by presenting a reinterpretation of the data set published by Corthésy et al. (1998). For a hypothetical circular shaft with a defined rock mass profile, it is illustrated how large-scale heterogeneities modify the induced stresses at the excavation boundary and thus affect longitudinal variations in the depth of failure. It is concluded that the combination of stress and strength heterogeneities leads to a highly variable excavation behavior with localization of various failure modes. Finally, it is demonstrated that the common assumption of far-field stress boundary conditions may lead to non-conservative model predictions when compared to far-field strain boundary conditions.

1 INTRODUCTION

Natural rock masses are heterogeneous in terms of modulus and strength. This paper was submitted in response to a call for contributions to the subject of "rock heterogeneity across all length scales" and to draw attention to the impact of rock mass heterogeneity on the in situ and excavation-induced stress field. In rock engineering, it is common practice to assume that the stress field is uniform and can be described by a single stress tensor. As a consequence, variations in excavation instability would have to be attributed to variations in rock mass strength alone. Experience by the lead author during a recent litigation case, which unfortunately cannot be published, has shown that the stress field was highly modified by rock mass strength and modulus heterogeneities and that the excavation behavior changed drastically as a result of this variability in strength and stress. Without reference to this particular case, simplified numerical (Voronoi) models, calibrated on published data (Corthésy et al., 1998), are used in the following to illustrate that:

- variations in field measurements can be attributed to rock mass stiffness variations;
- mining-induced stresses along an underground project can be highly varied; and the
- variability in excavation behavior has to be attributed to variations in both strength and stress.

In particular, it is demonstrated that heterogeneous rock masses, in terms of rock mass modulus, affect the local stress field differently under various far-field boundary conditions such as sedimentary, thermal, tectonic, and mining-induced strain boundary conditions.

1.1 Rock mass properties

The Geological Strength Index (GSI; Hoek et al. 1996) provides a means for obtaining the rock mass strength (Hoek-Brown parameters) as well as the rock mass deformation modulus (Hoek et al. 2002; Hoek and Diederichs 2006). Hence, the unconfined rock mass strength UCS_{rm} and the rock mass modulus E_{rm} can be related, as illustrated by Martin et al. (2003), and plotted in the UCS versus E space.

For the GSI-determined modulus, various relations have been established. Two are shown for undisturbed rock mass conditions (disturbance factor, D = 0) in Figure 1. The model by Hoek et al. (2002) provides linear trends whereas the model by Hoek and Diederichs (2006) results in curved trends. For the demonstrations in this paper, an artificial "randomized data set" (Figure 1) was generated by assuming normal distributions for the two parameters UCS and E: mean UCS_{rm} = 50 MPa and E_{rm} = 75 GPa with a coefficient of variation, CoV = 20% and 10%, respectively. Typically, the ratio E_{rm}/UCS_{rm} ranges from <1500 to >2500. For demonstration purposes, E_{rm}/UCS_{rm} of 1500 with a CoV = 10% is used here since this is in line with conditions applicable for the Canadian Shield. Hence, typical ranges for the two variables are: UCS_{rm} = 50±10 MPa (20% CoV) and E_{rm} = 75±7.5 GPa (CoV = 10%). Sheorey (1994) used an E_{rm} = 50 MPa for the uppermost layers of the earth crust in his elastic-static thermal stress model. This would correspond to a GSI of about 75. For very good quality rock masses, the E_{rm} could therefore be higher than assumed by Sheorey (a range in rock mass modulus is therefore used later in this article).

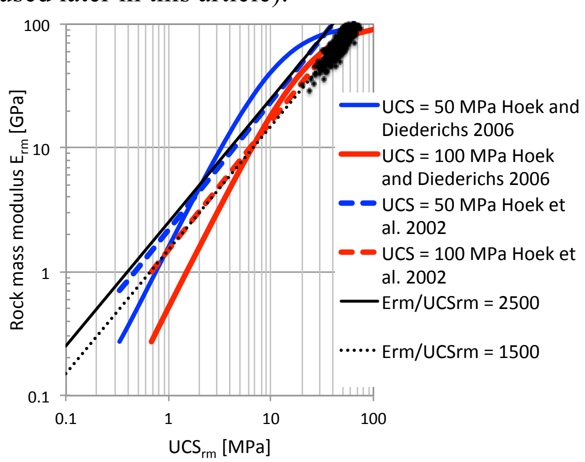

Figure 1 Rock mass modulus E_{rm} as a function of unconfined rock mass strength based on two GSI-modulus relations (for UCS = 50 and 100 MPa). See text for a description of the randomized data set.

1.2 Stress field simulation model

It is not or rarely possible to provide a truly representative discrete rock mass strength and modulus model at a global (km) scale. Hence, a Voronoi-tessellated model is adopted to explore the impact of rock mass strength and stiffness heterogeneity on the stress field for the following boundary condition scenarios:

I. Sedimentation scenario: no lateral movement during vertical stress increases due to material deposition.

II. Glacial loading scenario: addition of vertical surface stress due to ice surcharge with no lateral movement.

III. Tectonic straining scenario: horizontal displacement increments at the right model boundary while keeping the left boundary of symmetry fixed in the horizontal direction to generate a constant overall horizontal strain.

IV. Thermal straining scenario: addition of a horizontal displacement field at the right model boundary to represent Sheorey's (1994) elastic-static thermal stress model while keeping symmetry boundary on the left fixed as in Scenario III.

A 1 km wide and 2 km deep, heterogeneous rock mass volume was simulated using a randomly-shaped Voronoi-tessellation in RS2™ (or Phase2, version 9.0). RS2™ is a 2D finite element code developed by RocScience. The modeled geometry with a mean joint trace length of 20 m is shown in Figure 2a. The intact material properties used in the model (Table 1) were found to be suitable approximations for the site conditions presented by Corthésy et al. (1998). Their data will be analyzed later as a case example.

For the cases presented in this paper, one elastic and two plastic models are considered. The elastic model involves elastic Voronoi blocks and joints. The plastic homogeneous model consists of blocks and joints with identical properties whereas the plastic heterogeneous model considers identical joint properties but randomly assigned block modulus and strength properties. The properties of the Voronoi blocks and their boundaries (joints) are listed in Table 1.

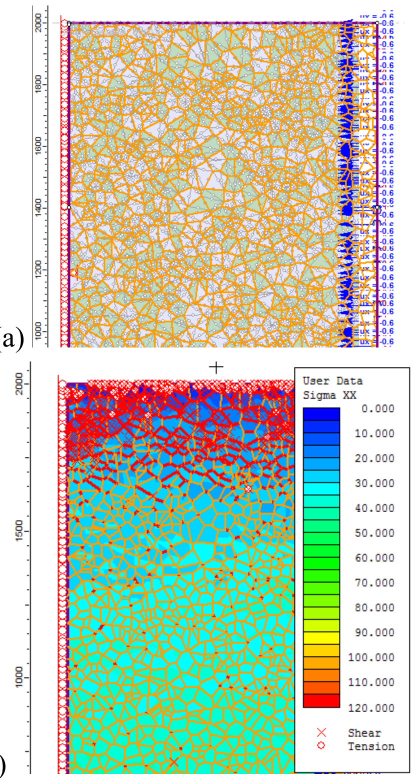

(a)
(b)

Figure 2 Voronoi model (only upper 1x1 km is shown) with parameters listed in Table 1: (a) Block geometry with two materials (50% each) and displacement boundary condition; and (b) horizontal stress distribution with yield pattern (red lines show slip on block boundaries; "x" and "o" represent shear or tensile failure of elements in blocks).

Table 1 Parameter set for models shown in this article.

	Joints	Blocks (50:50)	
c	0	-	MPa
phi	30	-	°
k_n	100	-	GPa/m
k_s	10	-	GPa/m
UCS_i	-	10; 150	MPa
m_i	-	5.7; 4.0	
E_i	-	30; 30 or 38	GPa
GSI	-	65; 55	

Note: the modulus of the simulated rock mass E_{rm} is lower than E_i, the modulus of the individual rock blocks, because of the joint stiffness and the joint frequency. Hence, the modeled E_{rm} is lower than the quoted moduli plotted in Figure 1. Since the strain-induced stress are proportional to the applied strain and rock mass modulus, lower strains and higher moduli produce identical results. Less applied strain therefore would produce identical stress profiles if higher stiffness parameters were used. However, the strain magnitudes applied to the models cannot be directly compared with actual strains encountered in the field.

Simulation of the various stress fields described earlier were implemented as sequential model stages. Accordingly, the vertical load and the lateral constraints were modified in stages:

- Stage 1: sedimentary condition with a prescribed stress ratio $k_o = \sigma_h/\sigma_v$; horizontal stresses are generated by Poisson's effect.
- Stage 2: glacial loading with a 20 MPa surface pressure applied with lateral constraints fixed at both vertical model boundaries in the horizontal direction.
- Stage 3: removal of the surface pressure and application of a horizontal displacement to cause a 0.02% overall horizontal strain.

The horizontal displacement (arrows in Figure 2a) was then incrementally increased to generate overall horizontal strain increments of 0.02%. In this article, Stage 5 (0.06% horizontal strain) and Stage 7 (0.1% horizontal strain) are examined in detail.

An overall strain increment of 0.02% causes a horizontal stress increment between 5 to 8 MPa for the adopted moduli in the model. Other combinations of strain and modulus would generate the same stress change. The above-described strain increment was chosen to investigate the evolution of the stress profile with increasing strain and to reach stress magnitudes typically encountered in the Canadian Shield (Corthésy et al., 1998). A typical model output is shown in Figure 2b with rock block and joint yield patterns as well as horizontal stress contours.

2 STRESS PROFILE SCENARIOS

In the following, horizontal and vertical stress profiles (stress versus depth) are presented for the various loading scenarios and illustrated in respective model outputs. The following stress designations are used: σ_v for vertical, σ_H for major horizontal and σ_h for minor horizontal stress. σ_z is used for the minor horizontal stress when σ_h is generated by plane strain condition in the 2D model.

While typical values reported for vertical stress gradients fall within a narrow range of 0.0265±0.001MPa/m for different geological settings (e.g., Martin et al., 2003 or Herget, 1988), horizontal stresses can vary widely depending on the geological, tectonic or thermal setting. For the horizontal stresses, the fitted trends are strongly influenced by the geology, the selected depth range and the adopted statistical method. The reported slope for linear fits to data range from <0.01 to >0.6, depending on the depth range and quality of the data. Such stress profiles are often practically meaningless without defining the applicable limits in terms of depth range and geological setting.

For example, linear projections of horizontal stress intercepts to the ground surface have been reported as 2.3 and 4.6 MPa (minor and major, respectively) for the Scandinavian Shield and as 5.4 and 10.1 MPa (minor and major, respectively) for the Canadian Shield (Martin et al., 2003). However, the apparent horizontal stress intercepts at the ground surface (depth z = 0) when considering only data from depths exceeding 600 m show values in the range of 10 to 40 MPa. Reasons for non-linearity in stress profile and for these differences in intercepts are discussed in Section 3.

Because linear trends tend to over-predict stress magnitudes at depth, which can lead to inappropriate stress assumptions for deep mines, asymptotic relations have been proposed (e.g., Corthésy et al., 1998; Martin et al., 2003; and others). Furthermore, because of stress relaxation effects near the surface, Maloney et al. (2006), building on findings from the Scandinavian Shield, demonstrated that it is often necessary to separately interpret data from shallow depth (<400 m; called Domain 1) and from greater depth (>600 m; called Domain 3). In between, typically from 400 – 600 m, there is a transition zone called Domain 2.

In the following, it is demonstrated that rock mass heterogeneity in different geological and tectonic settings influences the stress profiles with depth: both the variation in stress magnitude and gradient. The stress tensor orientation is also affected but this is not discussed here.

2.1 *Sedimentary scenario (Stage 1)*

For conditions of sedimentary deposition (Figure 3), the vertical and horizontal stresses (major and minor principal, respectively) are given by:

$$\sigma_v = \gamma z\,;\quad \sigma_H = \frac{\upsilon}{1-\upsilon}\gamma z \qquad (1)$$

where, z = depth in m and γ = average unit weight. The horizontal stress is a result of the laterally constrained Poisson's effect. For a Poisson's ratio ν = 0.33, the resulting in situ stress ratio $k_o = \sigma_H/\sigma_v$ is 0.5. The resulting vertical (black line) and horizontal (red line) stress profiles for the sedimentary scenario is linear with depth (going through zero at the surface at z = 0), as shown in Figure 3. The gradient of the vertical stress profile is defined by the unit weight of the rock and the gradient of horizontal stress as defined by the Poisson's ratio. Changes in the vertical stress gradient are caused by changes in the unit weight, but variations in the horizontal stress are primarily caused by variations in Poisson's ratio, as illustrated in Figure 3 for σ_H with a Poisson's ratio ν = 0.33 (red circles). For this example, with a simulated variability in Poisson's ratio using a coefficient of variation (CoV) of only 10%, the horizontal stress variations is >10 MPa below approximately 1000 m.

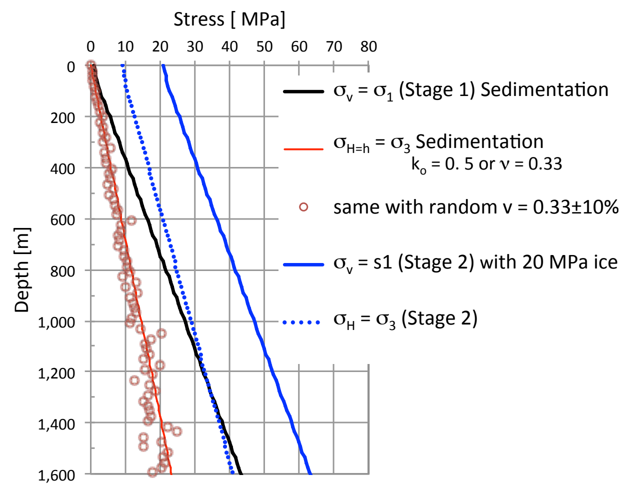

Figure 3 Stress profile for the sedimentary scenario Stage 1: vertical stress (black) and horizontal stress (red; with random ν as circles). Also shown are horizontal stress profiles for modeling Stage 2 after glaciation with 20 MPa ice load at the ground surface.

2.2 *Glacial loading (Stage 2)*

Glacial loading causes a shift of the vertical stress profile by the surface pressure (20 MPa in this scenario) and a shift of the horizontal stress profile by a constant (9.3 MPa in this case) that depends on the Poisson's ratio. The profile in Figure 3 was obtained by loading the model shown in Figure 2 with elastic properties following sedimentation in Stage 1. If the rock mass behaves in an elastic manner, the stress profile returns to the pre-glaciation Stage 1 upon glacial unloading. If the rock mass is plastically strained, residual stresses may be retained (not shown).

2.3 *Tectonic straining scenarios (Stages 3 to 7)*

The impact of horizontal straining (e.g., due to continental drift) is simulated next by assuming a constant horizontal strain profile. Horizontal deformation increments are applied to achieve an overall strain of 0.1% in increments of 0.02%, starting at Stage 3 after the removal of the glacial surcharge. Stages 5 and 7 represent overall horizontal strain cases of 0.06% and 0.1%, respectively.

A comparison of Figure 3 and Figure 4 shows that horizontal straining shifts the horizontal stress profile obtained from the sedimentary model by a constant increment that depends on the tectonic strain and the rock mass modulus. In the out-of-plane direction ($\sigma_z = \sigma_h$), the stress increment is lower due to the Poisson's effect alone (no tectonic strain is applied in the z-direction).

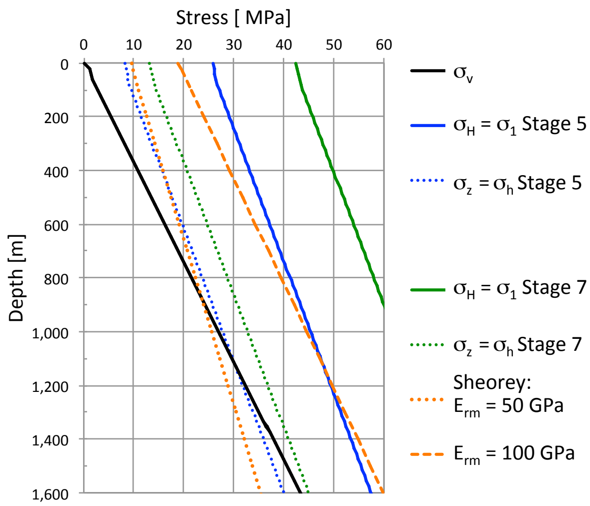

Figure 4 Stress profiles for homogeneous rock mass at 0.06% horizontal strain in blue (Stage 5) and 0.1% in green (Stage 7). Also shown are Sheorey's assumed stress profiles for E_{rm} = 50 and 100 GPa.

Due to the steeper gradient of the horizontal stress, compared to the vertical stress profile, the former may intersect the latter (e.g., at z = 1150 m for Stage 5 and >1600 m for Stage 7). At the depth of intersection, the intermediate principal stress (σ_h) will switch from horizontal to vertical or the vertical stress becomes the intermediate stress. This will be discussed in more detail later as the "flipping" of principal stresses renders many published principal stress trends invalid.

2.3.1 Profiles of stress ratio k

For the sedimentary scenario, the stress ratio k (σ_H/σ_v or σ_h/σ_v) is constant with depth (shown for k_o = 0.75 by black line) or slightly variable (shown for random Poisson's ration and k_o = 0.5 by red circles) due to variations in Poisson's ratio. The k-profile however assumes the familiar asymptotic shape (Figure 5) for tectonically or thermally strained conditions (imposed as constant horizontal strain in the simulations) for Stage 5 (blue) and Stage 7 (green). Also shown in Figure 5 are the limits (dashed and dotted black lines) for the large data set presented by Hoek and Brown (1980). The models at Stages 5 and 7 bound the upper limit of this data range.

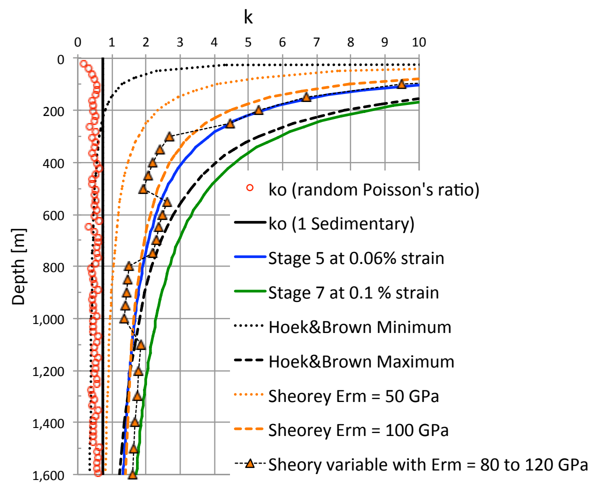

Figure 5 Stress ratio profiles for homogeneous rock at 0.06% horizontal strain in blue (Stage 5) and 0.1% in green (Stage 7) compared with relations developed by Sheorey and Hoek and Brown.

By applying a strain profile that linearly increases with depth from a non-zero horizontal strain at the surface, as proposed by Sheorey (1994; see Section 2.4), the k-profiles shown as dotted and dashed orange lines were obtained for E_{rm} = 50 and 100 GPa, respectively. These k-profiles fall in the center of the data range established by Hoek and Brown (1980). The corresponding horizontal stress profiles for these two rock mass moduli are also shown for comparison in Figure 4 (orange dotted and dashed lines). They show similar trends as the constant strain model for Stage 5 (σ_h and σ_H, respectively).

2.4 *Thermal straining scenario*

McCutchen (1982) explained the asymptotic k-profile with an isotropic spherical crust model assuming the crust is a non-compressible liquid.

Sheorey (1994) developed an elastic-static thermal stress model for the earth's crust and attributed the asymptotic k-profile to the earth curvature and the rock mass modulus. He proposed Eqn (2) to describe the k-profile as a function of depth (z) and rock mass modulus (E_{rm}).

$$k = 0.25 + 7E_{rm}(0.001 + \frac{1}{z}) \qquad (2)$$

The horizontal stress profiles corresponding to Sheorey's model for E_{rm} = 50, 100 and 150 GPa are superimposed on the graph produced by Maloney et al. (2006) in Figure 6 (orange lines) for comparison with data from the Canadian Shield.

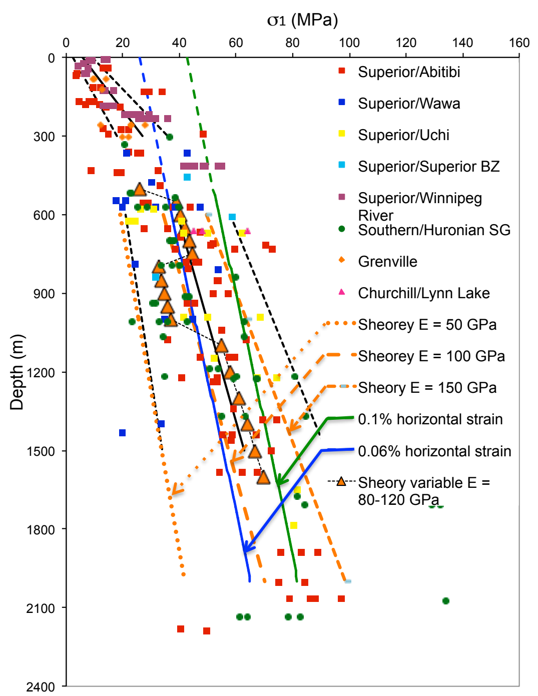

Figure 6 Reproduction of graph from Maloney et al. (2006) with profiles superimposed for Sheorey's model E_{rm} = 50, 100 and 150 GPa (orange) and the constant strain models with 0.06% (blue) and 0.1% (green) horizontal strain.

For the lower Domain 3 (below 600 m), the data trend with depth and the range are well represented by Sheorey's solution for E_{rm} ranging from 50 to 150 GPa. The central trend is also well represented by the RS2-model with a constant horizontal strain of 0.6% (blue line).

Most importantly, with respect to the influence of large scale heterogeneities on in-situ stresses and induced stress fields, Sheorey explained and provided an equation to obtain k and thus σ_H in bedded formations with different rock mass moduli. An example of a k-profile with inter-bedded layers with E_{rm} 80 and 120 GPa is shown in Figure 5 (orange triangles) to illustrate the effect of modulus variations on k.

The corresponding horizontal stress profile is presented in Figure 6 (orange triangles). This stress profile covers about half of the data range. A CoV in E_{rm} of about 30% would cover the entire data range. Sheorey's model demonstrates that rock mass heterogeneities in terms of rock mass modulus can strongly influence the stress profile. The effect of rock mass heterogeneities was also simulated using the RS2 Voronoi model and the results are presented in Section 3.

2.5 *Near surface stress relaxation*

Maloney et al. (2006) presented a "Reassessment of in situ stresses in the Canadian Shield" to assist in establishing representative in-situ stress conditions appropriate for sub-regional modeling. The in-situ stress model, comprised of three domains, describes the stress states in the upper 1500 m of the Canadian Shield. As in the Scandinavian Shield, the stress state in Domain 3 (below about 600 m) was found to be undisturbed when compared to the uppermost relaxed zones. Best-fit relations were established for this deep stress Domain 3 that are representative of the far-field stress condition. It is shown that the stress gradients at depth are much steeper than those obtained from gravitational gradients or from published data trends using a statistical fit to data from all three domains. They also pointed out that a wide scatter in stress magnitudes exists in the historical stress database.

Even after adding additional filtered data at greater depth, this scatter could not be much reduced and only slightly revised overall trends could be reported for Domain 3 (Yong and Maloney, 2015). Hence, factors that could contribute to the data scatter were explored and the findings are presented in this article. In particular, it is demonstrated how large-scale heterogeneities in deformation and strength properties of the rock mass contribute to, and often dominate, the scatter in in-situ stress magnitudes.

3 STRESS FIELD SIMULATIONS

Unrealistically high, i.e., infinitely high, stress ratios are predicted by elastic models because the rock at the ground surface cannot fail or yield. In reality, slip along faults or rock mass yield occurs during horizontal straining, which lowers the horizontal stress and thus the stress ratio. Thus, plastic models were run to capture the effect of joint slip and rock mass yield.

3.1 Homogeneous plastic model

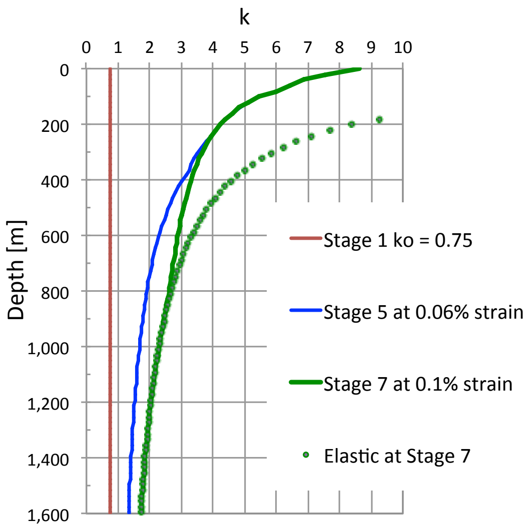

(a)

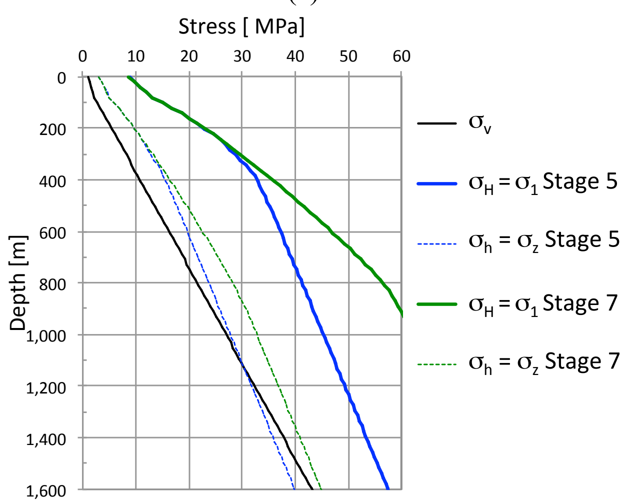

(b)

Figure 7 (a) Stress ratio k- and (b) horizontal stress profiles for homogeneous plastic model. Note: at 1100 m the vertical stress becomes the intermediate stress at Stage 5.

For the chosen rock mass parameters (Table 1), the near surface yield zone deepens (Figure 2) to about z = 400 m for 0.06% and to about 800 m for 0.1% overall horizontal strain. The corresponding k-, σ_H and σ_h profiles are shown in Figure 7.

The near-surface yield causes a horizontal stress relaxation and thus lowers the k-ratio (compare to elastic solution shown for 0.1% strain (green dots) or compare Figure 7a to Figure 5 or Figure 7b to Figure 4). The kink at about z = 100 m is an artifact resulting from the chosen block and element size.

The k-ratio drops from infinity to below k = 9 (Figure 7a) and the surface intercept for the horizontal stress drops in both cases to the simulated UCS of the rock mass (~9 MPa) and the initial slope flattens (Figure 7b). This is supported by the data shown in Figure 6. The shape at Stage 5 (0.06% horizontal strain; blue in Figure 6 and Figure 7b) corresponds well with the best-fit (mean) trend shown in Figure 6 (black lines).

The congruence of the data and model results suggests that the horizontal straining model is applicable for the Canadian Shield and supports the interpretation by Maloney et al. (2006) of the existence of two distinct domains (1 and 3) separated by a transition Domain 2. Near the surface, relaxation due to rock mass yield or slip on flat dipping structures characterizes Domain 1 (above about 400 m), whereas thermal or tectonic straining characterizes Domain 3.

3.2 Heterogeneous plastic model

The stress profiles for the heterogeneous model with two rock-block moduli, as described in Section 1.2 (Table 1), are presented in Figure 8 for Stages 5 and 7. Yielding of the blocks and joints near the surface and variations in block moduli causes wide variations in the horizontal stresses (σ_H and σ_h) when the heterogeneous rock mass is being strained. The yielding of blocks and joints controls the rock mass deformability near the ground surface and leads to a high variability in stress. As joint slip and yield is restricted or eventually prevented at greater depth, the variations are reduced significantly as it is then only controlled by the variations of the rock mass modulus. Hence, the highest variability in horizontal stress is to be expected in Domains 1 and 2 as illustrated by Figure 8.

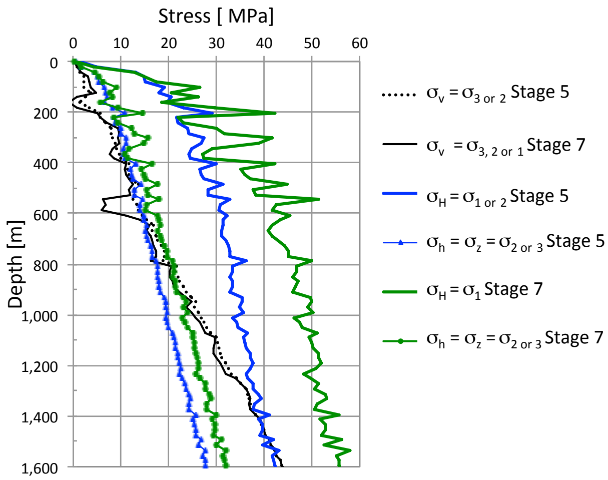

Figure 8 Vertical and horizontal stress profiles for the heterogeneous plastic model with 50% weak/soft and 50% strong/stiff blocks. Note: between 600 and 800 m the vertical stress becomes the intermediate stress and below 1600 m the major principal stress at Stage 5.

Figure 8 illustrates that all stress components are affected by the large-scale rock mass heterogeneity, particularly near the surface (to 600 to 800 m for the simulated case) where stress differences of more than ±10 MPa in σ_H and more than ±5 MPa in σ_h or σ_v can be observed for the chosen property range. The corresponding coefficients of variation are in the order of 5 to 10% near surface for this example. Below a depth of 600 m, the CoV drops to about 2 to 3%.

The data presented in Figure 6 again supports the results from the plastic heterogeneous and horizontally strained model. Only the vertical stress profile can be approximated by a linear trend. Both the minor and major horizontal stresses show a rapidly decreasing gradient near the ground surface (in Domain 1) with a transition to a linear trend with a stress intercept at the ground surface z = 0. For Stage 5, the intercept in the model measures 25 MPa for the major and 5 MPa for the minor horizontal stress (Figure 8). The lower intercept in the minor principal stress is a result of the assumed plane strain condition, i.e., a scenario with no tectonic or thermal straining in the out-of-plane direction. Because these values are higher than the reported intercepts (see introduction to Section 2), the overall horizontal straining in the Scandinavian and Canadian shields must be less than the overall strain applied in the model at Stage 5 (or the rock mass modulus is higher).

4 CASE EXAMPLE

In the following, the principal stress data presented by Corthésy et al. (1998), reproduced in Figure 9a, is reinterpreted within the framework of near surface rock mass yield and heterogeneity within a thermal or tectonic strain field. For this purpose, data points with unrealistic stress tensors were eliminated and the remaining data is plotted in Figure 9 with different size symbols for Domain 1 (smaller) and 3 (larger).

It is evident from Figure 9a and even more clearly from Figure 9b that this data set from the Abitibi region shows two distinct domains (above and below about 600 m). Hence, trend lines were generated for the principal stresses in the lower stress Domain 3. The equations for these trend lines are listed in Table 2. The trend lines for the vertical stress over the entire depth range is also shown and listed. The wide data scatter in relatively sparse data must be considered when comparing trend lines. Nevertheless, as will be evident later from the comparison with model predictions, the shown trend lines seem to be representative of the actual stress profile.

The slope of the vertical principal stress for the entire depth range is lower than expected for the vertical stress (0.021 instead of the expected 0.027). This can in part be attributed to some very low (even tensile) vertical stress data in the database (see Figure 9a) but also to stress tensor rotation. This is evident from the minor principal stress data fits shown in Figure 9b where the minor principal gradient below 600 m is very small (0.007), intersecting the vertical stress trend at about 700 m.

The slopes of the intermediate and major stresses are very similar at 0.013 and 0.012 (comparable to the gradient of 0.014 from the numerical model; see Figure 10).

As will be illustrated later, based on the numerical model, the vertical stress is the minor principal stress near the surface (to about 700 to 800 m for the RS2 model, see Figure 10) and then becomes the intermediate stress. Hence, fitting trend lines to minor principal stress values for the entire depth range is meaningless as it represents a fit to a mix of vertical and minor horizontal stresses.

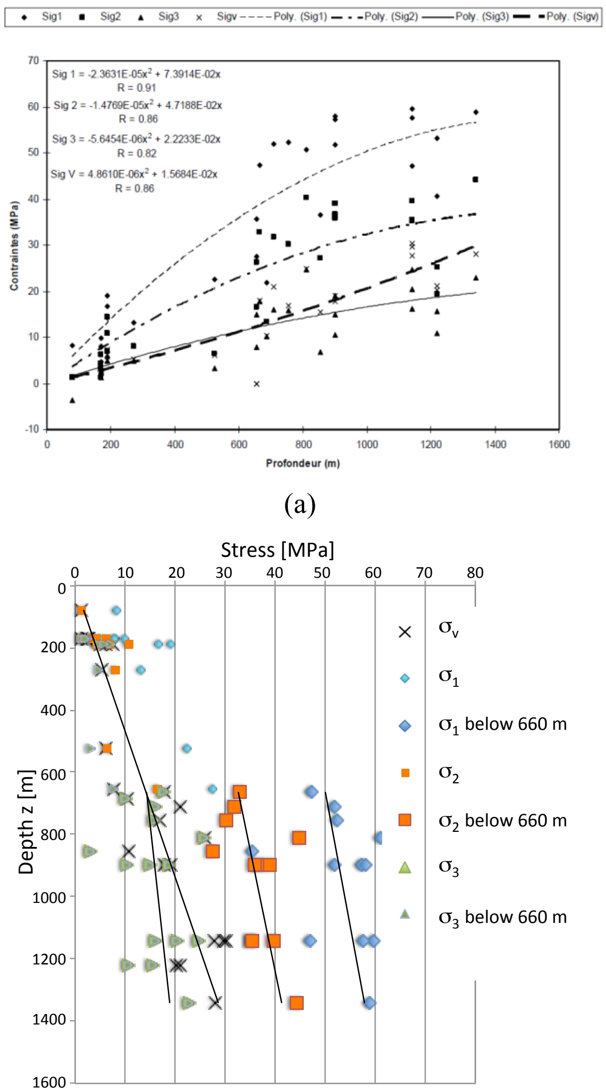

Figure 9 (a) Stress data near the Cadillac fault zone in the Abitibi area (Quebec, Canada) as interpreted by Corthésy et al. (1998); (b) reinterpreted data after separating data by domains (Domain 3 below 600 m; trend line data see Table 2).

Table 2 Equations for trend lines shown in Figure 9b.

$\boldsymbol{\sigma_v}$	= 0.021 z [m] for z = 0 - 1300 m
$\boldsymbol{\sigma_1}$	= 0.012 z +42.4 [MPa]; z = 660 - 1300 m
$\boldsymbol{\sigma_2}$	= 0.013 z + 24.1 [MPa]; z = 660 - 1300 m
$\boldsymbol{\sigma_3}$	= 0.007 z + 9.7 [MPa]; z = 660 - 1300 m

Note: slopes and intercepts are sensitive to individual data points.

The gradients of the three principal stresses are clearly steeper than that of the vertical stress and are more or less parallel with each other. These trends are roughly parallel to horizontal stress trends expected for a low $k_o < 0.5$ (see Figure 10) suggesting a constant shift by a more or less constant stress increment due to horizontal straining. Higher strains in the major principal direction cause a larger intercept (42 MPa) than in the intermediate stress direction (24 MPa).

A Voronoi model with higher rock mass and joint strengths, allowing yield to a depth of 400 m, is adopted to establish the trends for the Abitibi region (Corthésy et al., 1998).

The simulated stress profiles presented in Figure 10 are produced by a plastic, heterogeneous Voronoi model with a random rock mass modulus variation and deformed by constant horizontal straining.

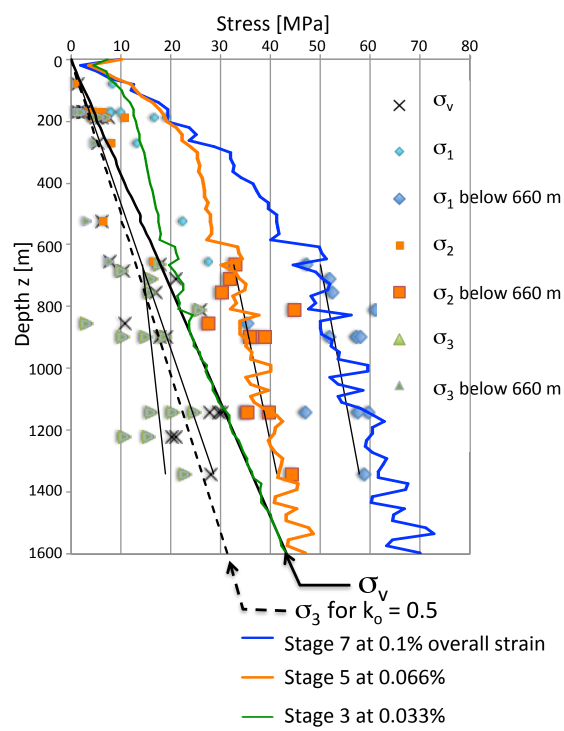

Figure 10 Reinterpretation of data from Corthésy et al. (1998) with a random rock mass modulus variation; three solutions for σ_H at 0.033 to 0.067 to 0.1% constant overall horizontal strain (green, orange, blue) are shown for heterogeneous, plastic rock block model.

This figure demonstrates that the data trends are well represented by a strained heterogeneous rock mass model. The measured gradients and range of variability in magnitudes correspond well; e.g., by comparing major principal stress measurements with modeled Stage 7. Only one measurement in Domain 3 falls outside the modeled range.

Several practically relevant observations can be made from this figure:

- With a few exceptions the trend and variability of $\sigma_{1=H}$ is almost perfectly matched by the 0.1% strain profile. The ultimate slope, below 1000 m, is steeper than the vertical stress gradient.
- The simulated profile with 0.066% horizontal strain follows the intermediate stress data below 600 m and again describes the variability well. This indicates that there is tectonic or thermal straining of different magnitudes in the two horizontal principal stress directions. The slope below 300 m is again steeper than the vertical stress gradient.
- The simulated profile with 0.033% horizontal strain demonstrates the earlier mentioned "flipping" of σ_3 from horizontal to vertical stress. The same would happen for the other profiles but at much greater depths (~2000 m for 0.066% strain).
- The simulated σ_h profile therefore falls below the vertical stress profile at about 700 m but follows the observed data trend. The assumed k_o = 0.5 may be slightly too high as most data points fall below the modeled trend line.

In summary, this reinterpretation of data from the Abitibi area confirms that the often measured stress variability is reality and can be attributed to rock mass heterogeneity; certainly in thermally or tectonically strained regions of the world. The principal stress gradients are steeper than the vertical stress gradients resulting in a "flip" in intermediate and minor principal stresses at some depth. Trend lines obtained from fitting minor and intermediate principal stresses may therefore be meaningless. Vertical and minor horizontal stresses must be grouped for trend analyses.

5 IMPLICATIONS FOR EXCAVATION STABILITY

The implication of stress variability on excavation stability is explored for a rock mass where brittle failure dominates and where Eqn (3) (Martin et al. 1999) for the estimation of the extreme depth of failure is applicable:

$$d_f/a = 1.25*\sigma_{max}/UCS - 0.51 \qquad (3)$$

where, d_f = extreme depth of failure; a = excavation radius; and $\sigma_{max} = 3\sigma_1 - \sigma_3$. The terminology "extreme" is adopted here because the data used for Eqn (3) includes only data from location where the largest, most extreme, depths of failure were recorded. The severity of excavation damage as described by Eqn (3) is therefore a function of the ratio of the mining-induced tangential stress σ_{max} and the rock's UCS.

For the example presented in Figure 8, the excavation-induced tangential stresses for a circular vertical shaft and for horizontal tunnels, excavated in the principal stress directions, at different depths are presented in Figure 11. Also, shown is the randomly generated UCS profile that will be used to estimate the depths of failure as a function of depth below ground surface. With a mean UCS = 125 MPa and a CoV = 20% the randomly generated UCS-values range from about 100 to 150 MPa (for 67% confidence).

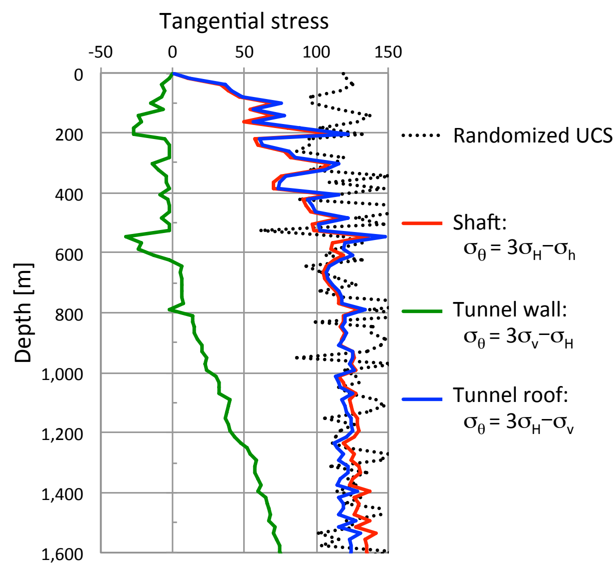

Figure 11 Tangential stress profiles for a vertical shaft (due to σ_H and σ_h); for tunnel roofs (due to σ_H and σ_v); and tunnel walls due to σ_H and σ_v. A randomly generated UCS profile for UCS = 125 MPa with a CoV = 20% is also shown.

The profiles of the induced depths of failure for the stress and UCS profiles presented in Figure 11 are shown in Figure 12 for a vertical shaft.

This figure highlights that a wide range in excavation damage must be expected due to the combined effect of stress and strength variation. At shallow depth, where UCS was assumed to be constant, the stress variability strongly influences the variability in the extreme depth of failure.

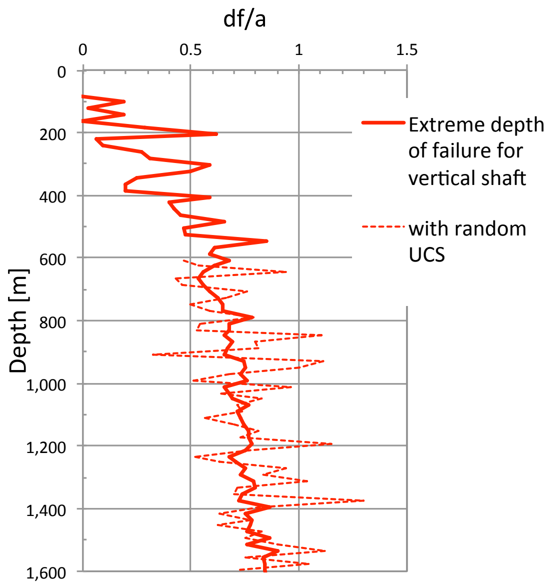

Figure 12 Extreme depth of failure profiles for a shaft with the stress profiles and randomized strength shown in Figure 11.

The impact of strength variability is only shown for depths exceeding 600 m. For this depth range, Domain 3, the variability due to stress is relatively low and the depth of failure gradually increases from about $d_f/a = 0.6$ to 0.8; i.e., between 3 and 4 m for a shaft with a diameter of 10 m. The UCS variability however dominates in Domain 3 and, as shown by one particular realization of a random UCS distribution, the anticipated extreme depth of failure varies between $d_f/a = 0.3$ and 1.3; i.e., locally up to 6.5 m for a 10 m wide shaft.

6 CONCLUSIONS

From the findings presented in this article, it follows that:

- Linear trends to stress data are only justified for sedimentary depositional environments.
- Stress data should be grouped by depth domains; only data from the undisturbed domain (called Domain 3 in this study) should be used to extrapolate to great depth (>600 m).
- The gradient of the minor and major horizontal stress profile is typically much steeper in Domain 3 than in the vertical stress profile. As a consequence, the major, intermediate and minor principal stresses may switch orientations (for examples see Figure 4, 7 or 10). In such cases, it is inappropriate to fit trend lines without considering stress tensor rotations.
- Stress variability can be attributed to rock mass heterogeneities that become dominant in conditions where the earth crust is thermally or tectonically strained. Strength and stiffness heterogeneity both strongly affect the variability in the in situ and induced stress profiles.
- At shallow depth, this stress variability tends to dominate tunnel stability by either causing relaxed conditions (Figure 11) or by generating rapid changes in the depth of failure profile (Figure 12).
- At depth, the extreme depth of failure still varies due to stress variability and gradually increases with depth. The variability in rock strength however tends to dominate the depth of failure at greater depth (Figure 12).

The findings presented in this article are of practical relevance for the design of underground excavations; particularly to those that cross heterogeneous rock mass domains.

Meaningful in-situ stress numerical models can be obtained for rock masses with large-scale rock heterogeneities by adopting horizontal strain rather than stress boundary conditions. As a matter of fact, the common assumption of far-field stress boundary conditions may lead to non-conservative model predictions when compared to far-field strain boundary conditions.

REFERENCES

1. Corthésy, R., D.E. Gill, and M.H. Leite 1998. Élaboration d'un modèle de prédiction des contraintes in-situ dans la région de la faille de Cadillac. CIM Bulletin 92(1020): 54-58.
2. Herget G. 1988. Stress in Rock. A.A. Balkema, Rotterdam, 179p.
3. Hoek E. and M.S. Diederichs 2006. Empirical estimation of rock mass modulus. International Journal of Rock Mechanics & Mining Sciences 43 203–215.
4. Hoek E., Carranza-Torres C.T., and B. Corkum 2002. Hoek-Brown failure criterion-2002 edition. Proc. of 5th North American rock mechanics symposium, Toronto, Canada, (1): 267–73.

5. Hoek E., P.K. Kaiser, W.F. Bawden, 1995. Rock Support for Underground Excavations in Hard Rock. A.A. Balkema, Rotterdam, 215 p.
6. Hoek E. and E.T. Brown1980. Underground Excavations in Rock. Inst. Mining & Metallurgy. London, 527 pp.
7. Martin C.D., P.K. Kaiser, R. Christianson, 2003. Stress, instability and design of underground excavations. International Journal of Rock Mechanics and Mining Sciences, 40(7-8): 1027-1047.
8. Martin C.D., P.K. Kaiser, D.R. McCreath, 1999. Hoek-Brown parameters for predicting the depth of brittle failure around tunnels. *Canadian Geotechnical Journal,* **36**(1): 136-151.
9. Maloney S., P.K. Kaiser, A. Vorauer, 2006. A Reassessment of in situ stresses in the Canadian Shield. Golden Rocks, Proceedings of 41st U.S. Symp. on Rock Mechanics (USRMS), Golden, Colorado, 9p, CD.
10. McCutchen W.R., 1982. Some elements of a theory for in situ stress. International Journal of Rock Mechanics and Mining Sciences, 19: 201-203.
11. Sheorey P. R., 1994. A theory for In Situ stresses in isotropic and transversely isotropic rock. International Journal of Rock Mechanics and Mining Sciences, 31(1): 23-34.
12. Yong, S. and S. Maloney, 2015. An Update to the Canadian Shield Stress Database. Report for Nuclear Waste Management Organization (NWMO), Report TR-2015-18, 23 p.